

Article

An Experimental Study of Heat Transfer in Pool Boiling to Investigate the Effect of Surface Roughness on Critical Heat Flux

Bashar Mahmood Ali 

Department of Construction Engineering and Project Management, College of Engineering, Alnoor University, Mosul 41012, Iraq; bashar.m@alnoor.edu.iq

Abstract: Utilizing pool boiling as a cooling method holds significant importance within power plant industries due to its ability to effectively manage temperature differentials amidst high heat flux conditions. This study delves into the impact of surface modifications on the pool boiling process by conducting experiments on four distinct boiling surfaces under various conditions. An experimental setup tailored for this investigation is meticulously designed and implemented. The primary objective is to discern the optimal surface configuration capable of efficiently absorbing maximum heat flux while minimizing temperature differentials. In addition, this study scrutinizes bubble dynamics, pivotal in nucleation processes. Notably, surfaces polished unidirectionally (ROD), exhibiting lower roughness, demonstrate superior performance in critical heat flux (CHF) compared to surfaces with circular roughness (RCD). Moreover, the integration of bubble liquid separation methodology along with the introduction of a bubble micro-layer yields a microchannel surface. Remarkably, this modification results in a noteworthy enhancement of 131% in CHF and a substantial 211% increase in the heat transfer coefficient (HTC) without resorting to particle incorporation onto the surface. This indicates promising avenues for enhancing cooling efficiency through surface engineering without additional additives.

Keywords: critical heat flux; heat transfer coefficient; pool boiling; surface roughness



Citation: Ali, B.M. An Experimental Study of Heat Transfer in Pool Boiling to Investigate the Effect of Surface Roughness on Critical Heat Flux.

ChemEngineering **2024**, *8*, 44.

<https://doi.org/10.3390/chemengineering8020044>

Received: 6 February 2024

Revised: 18 March 2024

Accepted: 8 April 2024

Published: 16 April 2024



Copyright: © 2024 by the author. Licensee MDPI, Basel, Switzerland. This article is an open access article distributed under the terms and conditions of the Creative Commons Attribution (CC BY) license (<https://creativecommons.org/licenses/by/4.0/>).

1. Introduction

In recent years, with the rapid advancement of knowledge frontiers and the consequent production of new products that work with extremely high heat loads, the need for an efficient and small heat exchanger, especially in microelectronic components, has been strongly felt, and this has created a stimulus and motivation [1–3]. Boiling helps to develop an effective technique to increase heat transfer, and it is more effective than single-phase heat transfer since the surface on which boiling occurs is in contact with a fluid of high latent heat that cools the surface more evenly and leaves no hot spots on it [4–6].

When the heat flux exceeds a certain value, a layer of vapor resulting from the joining of small bubbles and the production of a large overlying bubble covers the boiling surface and prevents heat exchange between the surface and the fluid (due to the lower heat transfer coefficient of vapor compared to water) [7,8]. In this case, the temperature jumps rapidly on the surface, and this can damage the boiling surface and the heater cartridge. This limiting point is called critical heat flux (CHF) in the boiling phenomenon [9]. If something causes a problem with the generation or the departure of bubbles on the boiling surface it is more likely to experience CHF [10].

Much research in boiling has been aimed at developing and enhancing the geometry of a particular surface to increase nucleation, reduce the surface superheat temperature, and delay the CHF [11–15]. A large number of methods are proposed, which are divided into active methods [16–19] and passive methods [20–22]. Passive methods include rough surfaces [23], porous and hydrophilic surfaces [24,25], nanoparticle addition to the base fluid [26–28], and surface expansion and using fins [29,30]. Active methods, however,

are mostly like creating an electrostatic field [31,32] and vibrating the surface and the boiling fluid [33,34]. In practice, the use of active methods in the industry is impractical or requires high costs [33]. The simplest way and passive method is to correct the surface by roughening it using machining and polishing with sandpaper. By roughening the boiling surface and causing cavities, the bubble trapping increases and the bubbles merge later, and the CHF is delayed [34].

Many attempts have been made to establish the correct relationship between the heat transfer coefficient (HTC) and the roughness. Also, there are many studies in which scientists have tried to tabulate and compare parameters with the experimental parameters. One of these studies is the work of Jones et al. [35]. The initial efforts on the surfaces to improve HTC were made by Jacob and Fritz [36]. In this study, the copper surfaces were roughened with grooves 1.6 mm deep with a step of 1.2 mm. The mentioned modifications led to an improvement in boiling HTC, where it became three times more than the smooth case. Berenson [34] managed to increase the HTC up to 6 times by polishing the surface by sanding it using different roughness. Also, according to the same study, from an amount of roughness onwards, no increasing trend was observed in heat flux. The effect of surface conditions had been ignored in most experiments and relationships until Ramilson [37]. With the help of his colleagues, he reported during his experimental study that the effect of wettability was more effective than the effect of surface roughness on CHF. Because the roughness only reduces the surface and bubble adhesion, and the bubble departs faster from the surface, the presence of micro-roughness on the surface prevents the bubbles from joining together quickly and increases the critical heat flux on rough surfaces. While the surface becomes hydrophilic, nucleation sites increase and the frequency of bubble generation increases and, due to the capillary state of nucleation sites, fluid is drawn into these cavities, the angle of impact of the droplet and surface decreases, and cavities and active nucleation sites are further fed by fluidization. This can lead to a further increase in CHF and HTC at the same time. Various methods have been proposed for the porosity of heat transfer surfaces, including chemical methods, roasting, electron washing, and deposition of nanoparticles on the surface. The formation of a thin, porous layer on the surface of the heater can significantly change the surface tension, wettability, surface roughness, density of active nucleation sites, and HTC. The creation of a porous coating on the surface has a strong potential to change the balance of forces in the triple line and the dynamic behavior of the bubble, such as the bubble detachment waiting time and frequency [38].

Kumar et al. [39] explored enhancing boiling heat transfer by modifying the surface properties of polished copper substrates with composite coatings of TiO_2 and SiO_2 nanoparticles. Surface characteristics were investigated for samples with varying coating durations. Results showed improved boiling performance with reduced onset of nucleate boiling temperature and enhanced heat transfer coefficients, peaking at around 10 μm coating thickness. Wang et al. [40] constructed an experimental rig to examine pool boiling heat transfer characteristics using R134a on both bare copper and Shieldex-coated surfaces with varied roughness. Findings indicated that surfaces with higher roughness generally exhibited higher heat transfer coefficients, with enhancements ranging from 5.2% to 75.5%. Dehkordi et al. [41] conducted a numerical study to examine how electric fields affected the dynamical behavior of $\text{H}_2\text{O}/\text{Fe}_3\text{O}_4$ nanofluid within an atomic microchannel. Using the LAMMPS package, simulations analyzed physical attributes like kinetic energy, potential/atom energy, and velocity profiles. Increasing the outer electric field accelerated the boiling phenomena in the nanofluid, revealing its significant influence.

The results of Souza et al. [42] on the effect of the deposition of $\gamma - \text{Fe}_2\text{O}_3$ nanoparticles with dimensions of 10–80 nm on a horizontal surface with a medium roughness of $R_a = 0.16 \mu\text{m}$ in the presence of HFE7100 as a working fluid showed that in the presence and deposition of small nanoparticles, compared with the non-settling surface of nanoparticles, an increase in the CHF and HTC is observed, while increasing the dimensions of nanoparticles at the same concentration causes the heat transfer coefficient to become less

than the non-settling surface. They attributed this decrease to surface insulation, a lack of cooling fluid penetration into the spongy tissue of the nanoparticles, and a decrease in the density of active nucleation sites. Gheitaghy et al. [43] electronically washed the polished copper surface in two stages, once with high duration and low current and again with short duration and high current applied to achieve greater strength of the layer. The images taken using a scan electron microscope (SEM) and static tests of the droplet and the surface showed that the electron-washed surface in their study was completely porous and hydrophilic, resulting in an increase in heat flux from 800 kW/m^2 to 1200 kW/m^2 . Narayan et al. [44] described the interaction of the surface parameter, which is determined by the ratio between the surface roughness and the average diameter of the nanoparticles. They reported that $SIP = Ra/dp > 1$ is the coefficient at which heat transfer occurs. The reason for this is that when the nanoparticles are smaller than the average surface roughness these nanoparticles settle into the cavity and turn an active cavity into several active sites, whereas in the presence of larger nanoparticles these nanoparticles reduce nucleation and bubble generation by covering cavities. The results of the study of the effect of porosity on the boiling surface over time by many researchers show that, in addition to the lack of strength of these deposited layers and separation from the boiling surface at high heat fluxes, another disadvantage of such coatings is due to hydrophilicity. With increasing fluid penetration into the cavities, the air is slowly degassed from the cavities and the active cavities are completely filled by the working fluid over time and lose the ability to produce bubbles; thus, these improvements in the boiling properties do not last long [45]. Ahmed and Hamed [46] reported that the thickness of the settling layer on the surface during the nanofluid boiling process is proportional to the concentration of nanoparticles in the fluid; as the concentration of nanoparticles increases, the settling rate increases and the HTC decreases. The setting layer is deposited by nanoparticles with low concentration, which increases the HTC. Gheitaghy et al. [47], by creating U-shaped microchannels and combining the method of increasing the surface area via microchannels and porosity of the surface via electron washing process, tested the pool boiling in the presence of deionized water. In this way, they practically combined passive methods of increasing the heat transfer surface, thereby creating a vapor-fluid passage path and creating more nucleation sites. The results of their experimental studies showed that the heat flux reached 1650 kW/m^2 and the heat transfer coefficient reached $225 \text{ kW/m}^2\text{K}$, which increased the heat flux by 100% compared to the polished surface of copper and HTC by about 80%. Increasing the level of heat transfer by creating microchannels and combining them with the boiling phenomenon is very interesting. Expanded surfaces provide a separate path and passage for fluid and vapor to pass through, in addition to increasing the surface area of the heat transfer surface to dissipate high heat fluxes from low levels. By creating a microchannel surface with short-length channels on the copper surface, Jaikumar and Kandlikar [48] were able to increase the heat loss rate to 2400 kW/m^2 in the presence of water as the working fluid, which, compared to the polished copper surface, showed a 120% increase in CHF. By creating microchannels on the copper surface and by making only parts of the wall porous, not the whole surface of the microchannel, Jaikumar and Kandlikar [48] succeeded in increasing the heat flux to 3250 kW/m^2 and heat transfer coefficient to $565 \text{ kW/m}^2\text{K}$, which resulted in an unprecedented 782% increase in HTC.

Despite the use of the roughening method by many researchers and many studies on the effect of roughness on the CHF and HTC, it seems that, so far, only a few studies have been devoted to the orientation and movement of sandpaper on the surface and its effect on fluid and bubble dynamics in delaying the CHF. This method is also suitable for improving surface properties in terms of the simplicity of production, cheapness, and duration of stability in the boiling process and can be focused on as an efficient method in the industry.

In this research, after making a pool boiling machine and polishing the boiling surface using 1500-tooth sandpaper, the pool boiling test was performed in the presence of water fluidization. In order to evaluate the accuracy and validity of the data extracted in the present study, the data were compared with experimental equations and experimental

data from other researchers. In the continuation of the experiment, circular micro-grooves were created on the copper surface by CNC machining and polishing the surface with 600-tooth sandpaper in a circular manner. Water was tested on these two surfaces, and the bubble dynamics and the amount of heat flux were compared with the previous state. The surface was again investigated and machined to create 13 microchannels with trapezoidal cross-sections to investigate the effect of increasing the surface and creating a rotational flow and its effect on the swaying of bubbles and creating a path to separate the downward fluid from the upward hot bubble. Finally, the heat flux and heat transfer coefficient in the presence of microchannels were investigated, and a general comparison of all models is performed. The novelty of the current research is that it has investigated the heat transfer coefficient and critical heat flux for surfaces with various roughness and a surface with microchannels. This research compares the results of these cases and shows how CHF and HTC increase by modifying the surface of boiling.

2. Materials and Methods

As shown in Figure 1, the device built to perform the pool boiling test consists of four main parts. The first part is the boiling part of the device, which contains the boiling chamber, heater cartridge, insulators, and holding frame. The second part is the cooling part of the device, which includes the helical condenser, the coolant tank, the pump, and the hose. The third part is the control part of the device, which consists of a thermostat, safety valve, pressure gauge, multimeter, and VARIAC autotransformer. The fourth part is the sensitive part of data collection, which includes thermocouples, DAQ data cards, a computer, and a high-speed camera with LED lamps.

The boiling part of the device is made of borosilicate glass that is able to withstand high thermal stresses and is also transparent so that the flow and phenomenon of boiling can be photographed and observed (height 300 mm, outer diameter 200 mm, thickness 5 mm). Also, the glass is completely insulated by fiberglass and a reflective coating so that the temperature of the boiling fluid does not drop rapidly from saturation. At the two ends of the Pyrex cylinder, silicone O-ring seals are placed and secured using thermal adhesive and, from above and below, RTV silicon droppers with a heat tolerance of 300 °C are stuck to two anti-acid steel (Steel-316) plates with dimensions of 300 × 300 mm² that have been thoroughly polished to prevent water and steam from leaking into the environment. There are three holes in the center of the steel, which are the location of the boiling surface, the tank drain valve, and the 500-watt preheater heater. The heater cartridge is copper due to its high thermal conductivity and good machining. The cartridge, as shown in Figure 1, is made of a cylinder with a diameter of 40 mm and a length of 300 mm. The geometry of the block is designed so that the heat transfer is closer to one side. The heater cartridge houses three K-type thermocouples and an RTD-Pt100 resistance sensor. At the end of the copper cartridge, there is a place for a steel heater (20 × 200 mm²) with a power of 2000 W. The boiling chamber and the upper and lower steel surfaces are placed on a metal frame to prevent vibration and movement of the device during boiling.

Also, in order for the boiling surface to be completely horizontal and level, the support frame of the device has height-adjustable bases. In order to minimize heat loss around the copper cartridge, assuming one-dimensional heat transfer in the direction of the heater cartridge, and to ensure the estimate of the surface temperature is correct and valid, combined insulation around the cartridge is used. A ceramic cylinder is prepared, and a heater cartridge is placed inside it. The initial layers around the ceramic cylinder are covered with rock wool insulation, and the next layers are covered with fireproof glass wool insulation. When insulating, care must be taken not to compress the insulation, because if the interstitial air of the insulation is compressed and released the efficiency of the insulation can be reduced by up to 50%. At the end of the insulation, the outer surface of the insulation is covered with a Teflon sheet and a reflective coating. The upper part of the heater cartridge, which is in contact with the boiling fluid, uses Teflon PTFE thermal

insulation, according to Figure 1, which has a much lower thermal conductivity and less adhesion than copper ($K_{copper} = 400$, $K_{PTFE} = 0.25$ W/mK).

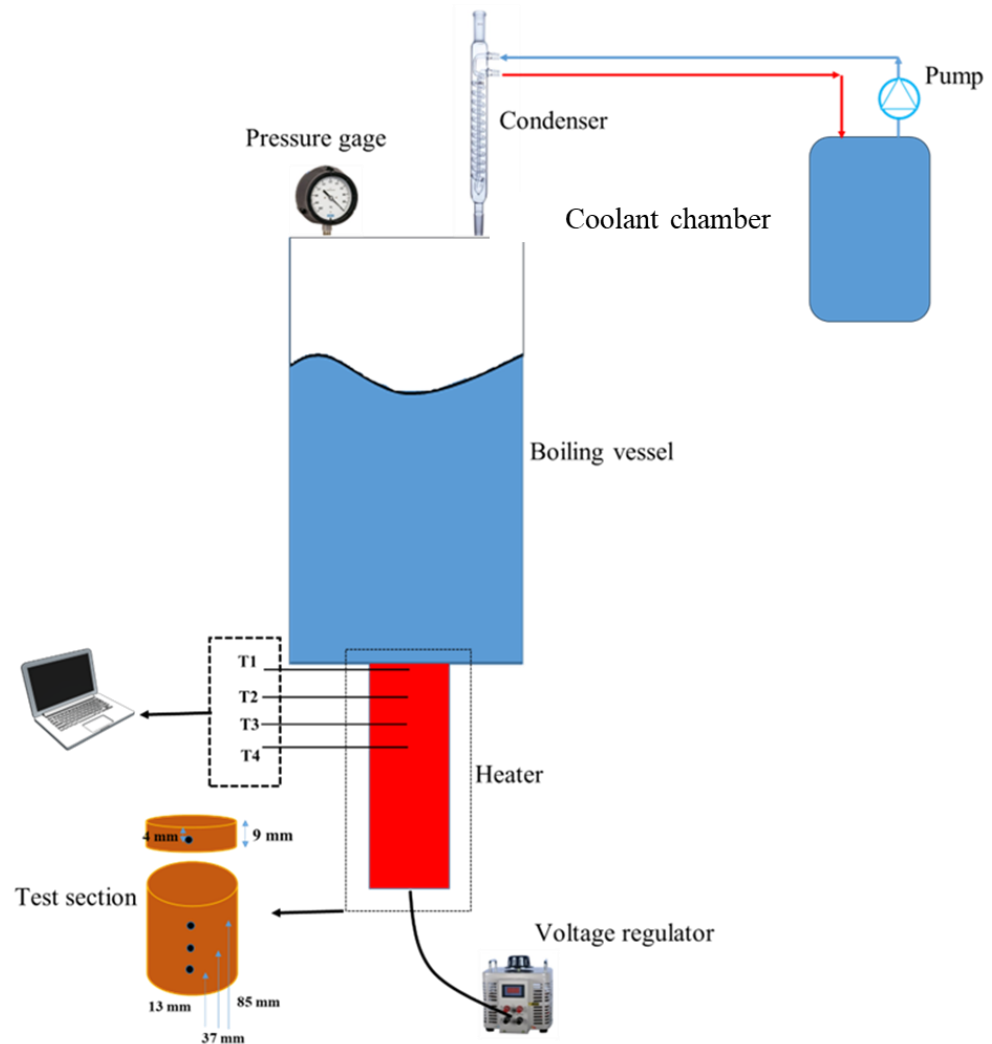


Figure 1. The experimental setup.

For this purpose, vapor condensation and keeping the volume constant are important points. A spiral condenser is used at the top of the boiling chamber. This condenser is connected via a hose to a pump with a flow rate of 400 L per hour, which is located in a 12 L coolant chamber. All connections, the coolant tank, and the boiling chamber are insulated with rock wool and aluminum foil to reduce heat loss.

In the control part of the device, an in-water heater is used to always keep the fluid inside the chamber in a saturated state. This heater is connected to the thermostat of the Atonics-TCN4 model; whenever the temperature of the fluid drops slightly, it is turned on with the command of the secondary heater thermostat, and the fluid temperature is returned to saturation. The temperature at the test site was 23 °C and, due to the effect of the altitude, the pressure was 80 kPa, so the boiling temperature of the fluid was approximately 94 °C. To control the pressure inside the boiling chamber, a pressure gauge is used, and a calibrated safety valve is used to discharge the excess steam generated into the environment and return the pressure inside the chamber to atmospheric pressure. It is important to note that all the experiments were carried out in 1 atm. A VARIAC autotransformer with 3000 W power is used to increase the heater voltage gradually. This VARIAC is connected to a multimeter to record the voltage and current of each step (for constant conditions in all tests).

The most important part of the device is the data collection section. This part includes 6 thermocouples (3 K-type thermocouples and 3 three-wire resistance sensors Pt100) with a thickness of 5 mm, and all thermocouples are calibrated in a constant temperature bath and have an accuracy of ± 0.1 °C. In order for the wires of the thermocouples to have good temperature resistance and also not to disturb each other due to the proximity of the sensors in the heater cartridge, the sensor wires are made of Teflon. A silicon paste with a thermal conductivity of $K = 4.5$ W/mK is used for proper contact and heat transfer between the steel body of the thermocouples and the heater cartridge. All thermocouples are connected to a 6-channel vector data card. The Pt100 sensor is located 4 mm below the boiling surface due to its higher accuracy and is used to estimate the surface temperature. Two thermocouples are also used to calculate the temperature of fluid saturation at the boiling point at two different heights inside the boiling chamber. The thermocouples are located at the bottom of the chamber and approximately at the free surface of the fluid. An LED lamp is installed at the top of the boiling chamber to facilitate the ability to shoot high-speed videos.

Uncertainty Analysis

With proper insulation around the heater cartridge, radial heat transfer to the environment can be avoided and heat transfer can be considered one-dimensional. Therefore, in order to obtain and estimate the surface temperature, assuming that heat transfer is one-dimensional, we can use Equation (1) of Fourier's law of thermal conductivity and obtain the heat flux.

$$q'' = K \frac{\partial T}{\partial Z} = K \frac{T_4 - T_1}{Z_4 - Z_1} \quad (1)$$

In a heat flux with a constant q'' and a constant coefficient of thermal conductivity of copper, it is concluded that the temperature gradient remains constant in terms of height.

$$\frac{\partial T}{\partial Z} = cte = a \rightarrow T = az + b \quad (2)$$

An RTD resistance sensor with a high accuracy of ± 0.1 °C is placed 4 mm below the boiling surface to estimate the boiling surface temperature; by using the method of fitting a line between the temperatures according to Equation (3), the surface temperature can be estimated with good approximation.

$$T_s = T_1 - \left(\frac{q'' Z_1}{K} \right) \quad (3)$$

where Z_1 is 4 mm, based on Figure 1. To calculate the temperature of the boiling fluid, two Pt100 sensors are used, which are waterproof-insulated and installed at two heights, one on the fluid surface and the other near the boiling surface. Having the surface temperature and the temperature of the working fluid, according to Equation (4), the difference in the surface superheat temperature can also be determined.

$$\Delta T = T_1 - \left(\frac{q'' Z_1}{K} \right) - T_{sat} \quad (4)$$

The heat transfer coefficient on the surface and in the fluid are also calculated according to Equation (5).

$$HTC = \frac{Q/A}{T_s - T_{sat}} \quad (5)$$

Two types of errors often cause experimental data to differ from the actual values—measurement error due to non-calibration of measuring devices and equipment and human errors. Moffat's method [49] is used to calculate the uncertainty in the pool boiling test. The heat flux depends on the heat transfer coefficient of copper and the temperature

difference and location of the thermocouples. The thermal conductivity of copper is about 401.6 W/mK at 100 °C and about 400 W/mK at 300 °C. So,

$$\Delta K_{cu} = K_{100} - K_{300} = 401.6 - 400 = 1.6.$$

The uncertainty error of the thermal sensors is about ± 0.1 °C and, since the holes where the thermocouples were placed were produced by the CNC machining process, the distance between the holes is relatively accurate—they have an error of less than ± 0.1 mm.

$$q'' = f(K, \Delta T, \Delta Z)$$

$$\frac{U_{q''}}{q''} = \sqrt{\left(\frac{U_{T_4-T_1}}{T_4-T_1}\right)^2 + \left(\frac{U_{Z_4-Z_1}}{Z_4-Z_1}\right)^2 + \left(\frac{U_K}{K}\right)^2} \quad (6)$$

$$T_s = f(Z_1, q'', K)$$

$$\frac{U_{\Delta T_s}}{\Delta T_s} = \sqrt{\left(\frac{U_{T_1-T_{sat}}}{T_4-T_{sat}}\right)^2 + \left(\frac{U_{Z_1}}{Z_1}\right)^2 + \left(\frac{U_K}{K}\right)^2} \quad (7)$$

$$HTC = f(q'', \Delta T)$$

$$\frac{U_{HTC}}{HTC} = \sqrt{\left(\frac{U_{q''}}{q''}\right)^2 + \left(\frac{U_{\Delta T_s}}{\Delta T_s}\right)^2} \quad (8)$$

Based on the accuracy of the measuring device in the above method, the maximum error in calculating the heat flux and heat transfer coefficient is 6.3% and 9%, respectively. The shorter the distance between the thermocouples and the lower the difference in temperature, the greater the uncertainty. As the heat flux increases, the temperature difference increases, resulting in a decrease in the percentage of uncertainty. In Figure 2, this error in heat fluxes is higher than 500 kW/m² and reaches as low as 1.4% for calculating the heat flux and 2.8% for HTC.

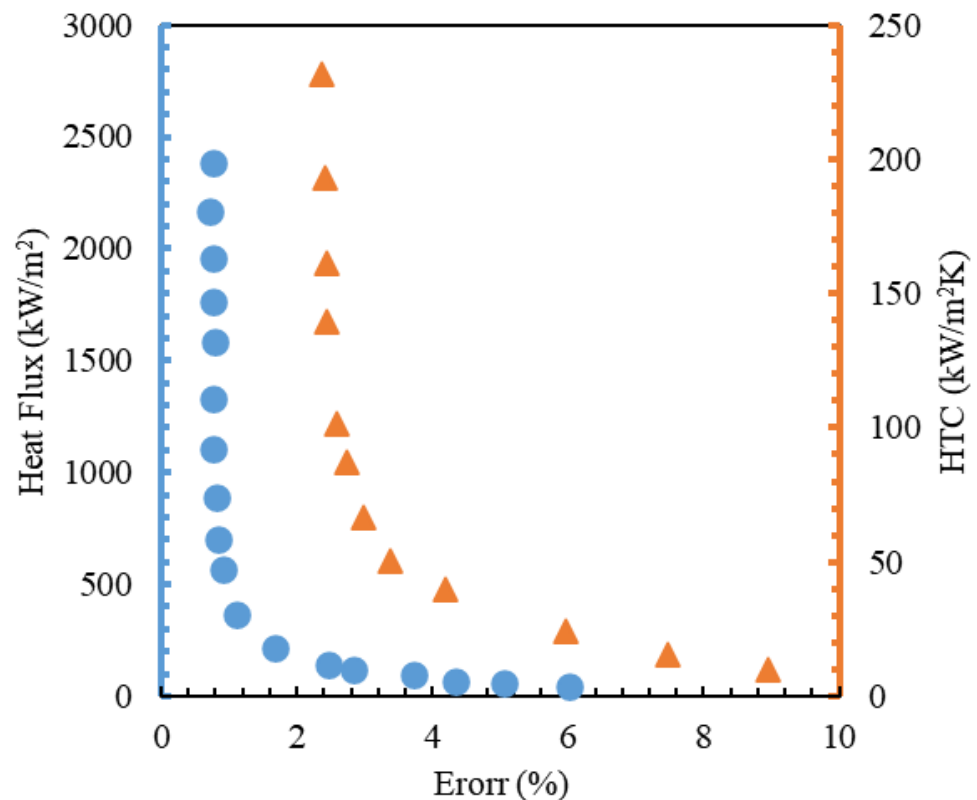


Figure 2. Uncertainty of HTC and CHF.

Also, Table 1 demonstrates the uncertainty of the measurements in the present study.

Table 1. Uncertainty calculation of experimental data.

Parameter	Uncertainty
Sensors (K)	±0.1 °C
Voltage (V)	±1%
Current (A)	±0.1%
HTC (kW/m ² K)	±6.3%
CHF (kW/m ²)	±9.6%
Surface temperature difference (K)	±9%

3. Results and Discussion

Pool Boiling Test of Various Surfaces in the Presence of Water

In the first part of the experiment, the boiling surface after machining was thoroughly polished with 1500-tooth sandpaper. The polished surface was washed using deionized water, linen cloth, and acetone to remove any grease and contamination from the copper surface. The surface roughness of the polish was measured using a roughness tester. In order to perform the boiling test, first, the heater cartridge was preheated, and then 3 L of deionized water was poured into the boiling chamber. At the same time, the water heater was turned on in order to keep the working fluid saturated. After visual inspections based on fluid degassing and the absence of suspended bubbles in the fluid, the activity of the condenser, in order to condense the vapors resulting from boiling, was instigated. In the case of convective heat transfer, the VARIAC was increased in 15-volt increments; in the boiling stages by 10 volts; and near the critical point the VARIAC power was increased by 5 volts. A steady state was considered to occur for each step when all sensors did not change by more than 0.1 °C for 10 min. In this research, the accuracy of the extracted data has been investigated in three ways.

- (A) Comparison of data with experimental relationships in the field of boiling;
- (B) Comparison with the results of experimental data of other researchers in this field;
- (C) Holding a repeatability test.

Before testing on different types of surfaces, experiments were performed using distilled water as the operating fluid on the surface with a roughness of 0.114 μm to check the accuracy and precision of the device. Then, the experimental results were compared with the experimental models presented by Rohsenow [50] and Gorenflo [51] according to Equations (9) and (10).

$$\frac{C_{p_l} \Delta T}{h_{fg} Pr^1} = C_{sf} \left[\frac{q''}{\mu_l h_{fg}} \sqrt{\frac{\sigma}{g(\rho_l - \rho_g)}} \right]^{0.33} \quad (9)$$

where ΔT is the superheat temperature, C_{p_l} is the heat capacity of the fluid, h_{fg} is the enthalpy of evaporation, Pr is the dimensionless Prandtl number of the liquid phase, C_{sf} is the coefficient of surface and fluid correction, q'' is the heat flux, μ_l is the viscosity, and σ is the surface tension.

$$\frac{h}{h_0} = F_{pr} \left(\frac{q''}{20,000} \right)^n Ra^{0.133} \quad (10)$$

In Equation (10), R_a is the mean roughness and h_0 for the working fluid is 5.6 kW/m² [51]. The pressure correction coefficient, F_{pr} , and n are calculated from Equations (11) and (12).

$$F_{pr} = 1.73 \left(\frac{P}{P_{cr}} \right)^{0.27} + \left(6.1 + \frac{0.68}{1 - (P/P_{cr})} \right) \left(\frac{P}{P_{cr}} \right)^2 \quad (11)$$

$$n = 0.9 - 0.3 \left(\frac{P}{P_{cr}} \right)^{0.3} \quad (12)$$

As can be seen in Figure 3a, the results of the boiling test are relatively consistent with the proposed models. In addition, in Figure 3b, the results are compared with the work presented by other researchers in this field and show good agreement. In order to verify the data presented, which are dependent on the environmental conditions of the experiment, the experiment was conducted over two different days, as shown in Figure 3c. The extracted results indicate a small and acceptable deviation in the data. By performing these three comparisons in the validation of the device, it was found that the validity of the data was accurate and reliable.

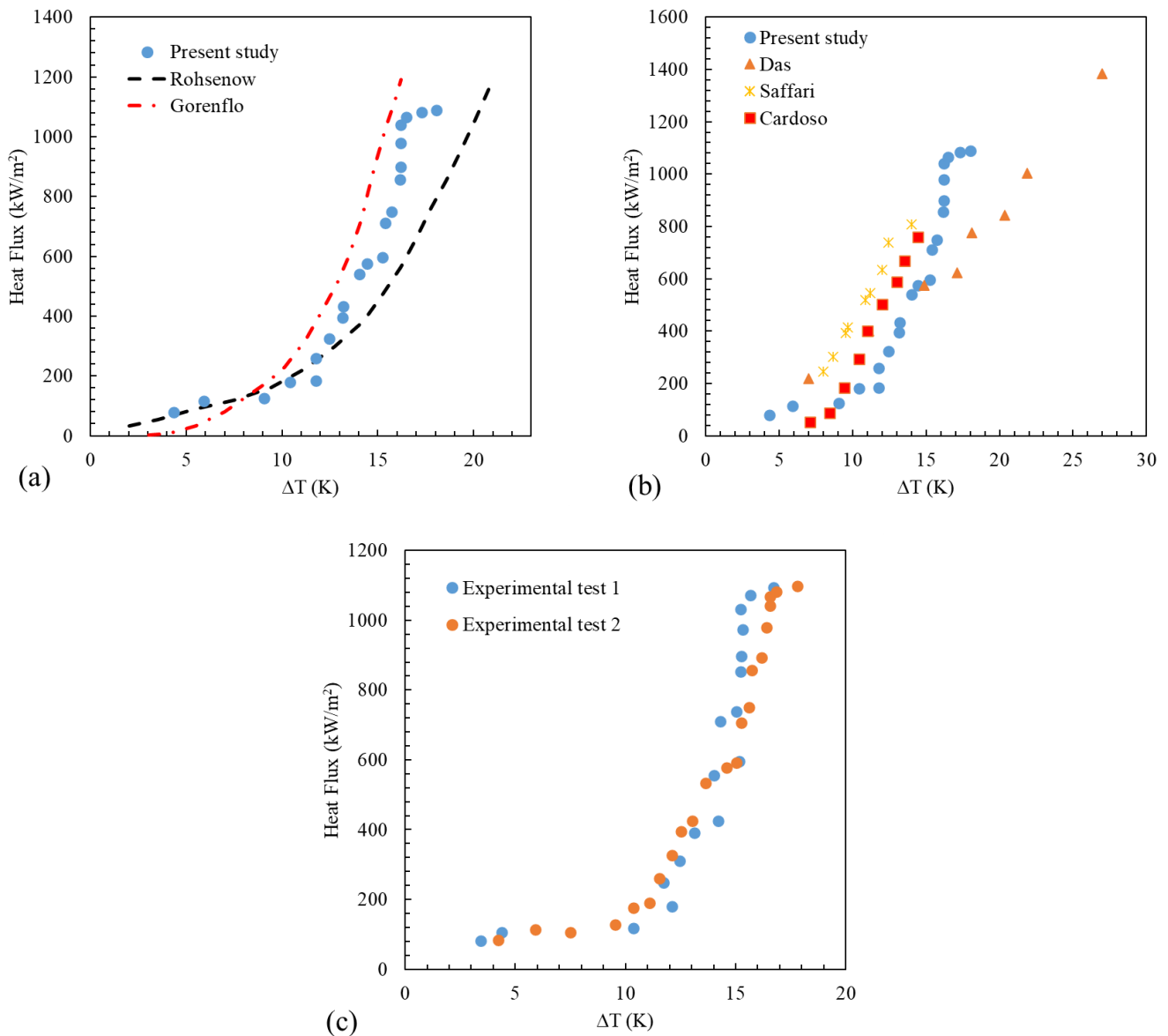


Figure 3. A comparison of the results with experimental relations [51] (a), other research [52–54] (b), and repetition experiments on two different days (c).

In the first experiment, the phenomenon of pool boiling on a polished surface with an average roughness of $0.06 \mu\text{m}$ was investigated. By performing experiments on this surface in the presence of 3 L of deionized water, the heat flux diagram was drawn in terms of the surface superheat temperature and heat transfer coefficient, as shown in Figure 4 of the SEM images taken from the polished surface. The level of roughness and density of nuclear sites was low. As a result, the surface does not have the ability to produce and respond to

the large volume of bubbles produced, and the bubbles connect very quickly to each other, producing bubbles that cover the surface.

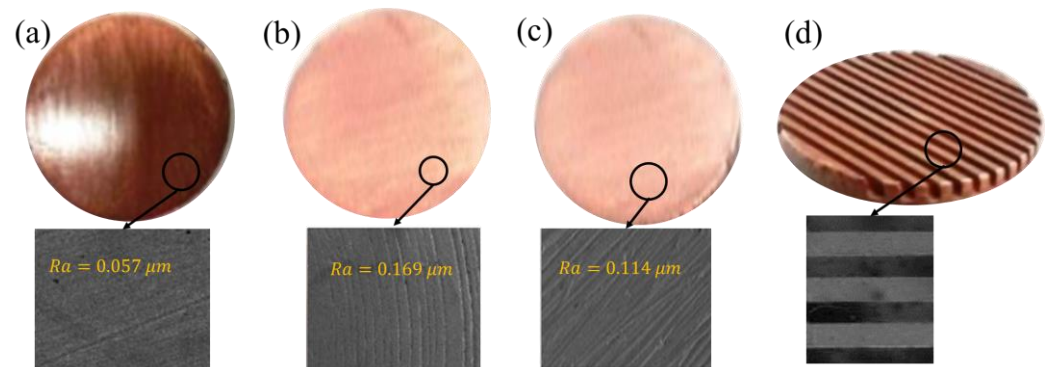


Figure 4. The four different boiling surfaces with their SEM images, (a) polished surface, (b) the rough surface in a circle, (c) the rough surface in one direction, (d) the microchannel.

According to Figure 5, the surface reached a maximum heat flux of 791 kW/m² and a heat transfer coefficient of 44.5 kW/m²K at a superheat temperature difference above 20.23 K. In the continuation of the experiment, the surface was rotationally roughened using a CNC lathe. As shown in Figure 4b, by polishing the produced surface in a circular shape (RCD) using 600-tooth sandpaper, a surface with a much higher surface density and roughness could be produced. Increased surface roughness results in smaller bubbles and these micro-dimensional peaks and depressions on the surface prevent the insulating bubbles from adhering rapidly to the surface and retaining their bubble separation ability up to higher fluxes than the polished surface test.

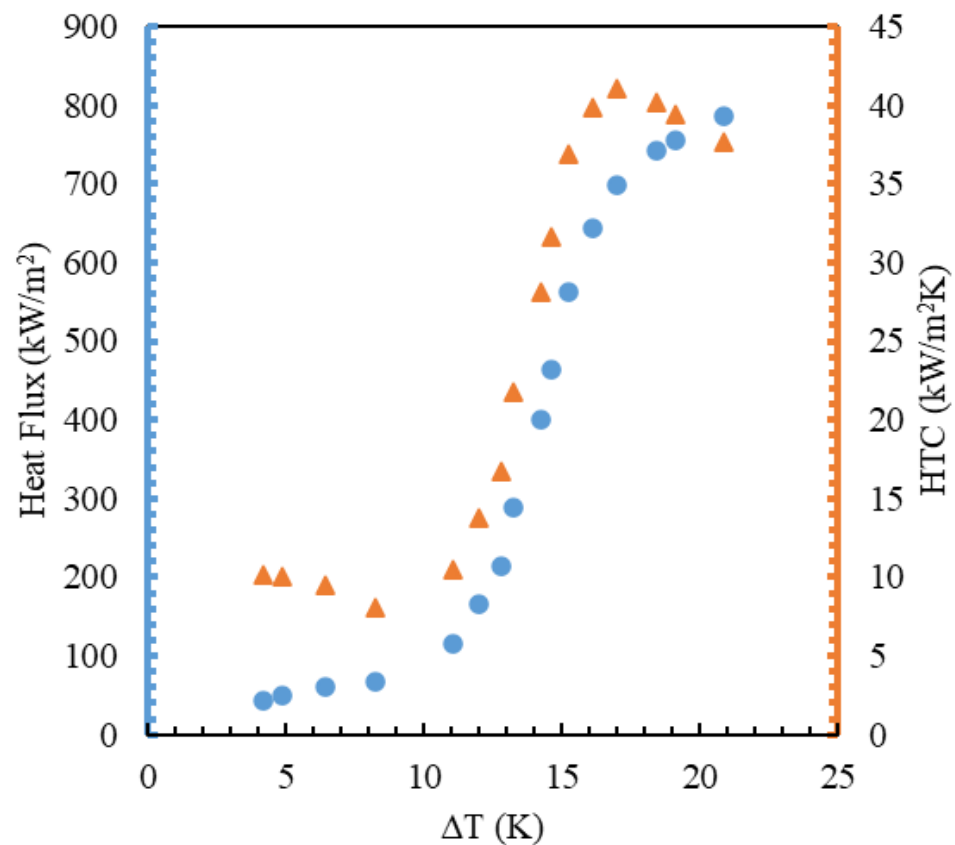


Figure 5. The graph of HTC and CHF of PS.

By performing the pool boiling test in the presence of this surface, as in Figure 6, the results show that the maximum heat flux increased by 903.74 kW/m²K and the heat transfer coefficient increased to 53.2 kW/m²K. It was important to note that the surface superheat temperature difference in the critical heat flux reached 18.84 K, indicating that the heat flux diagram was shifted to the left and that at a lower superheat temperature a higher heat flux occurred relative to the polished surface, which indicates an increase in surface efficiency.

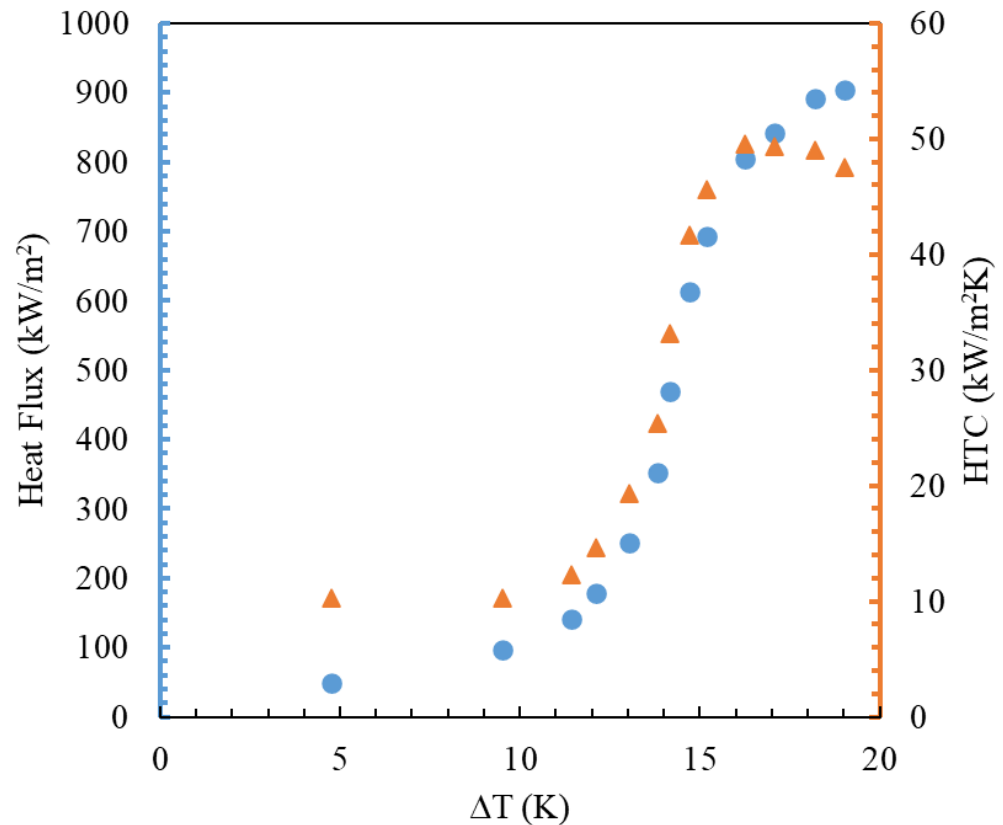


Figure 6. Results of CHF and HTC in RCD.

In the next experiment, the surface was polished using 600-tooth sandpaper in one direction (ROD) (Figure 4c); the pool boiling test was performed in the presence of this surface and the deionized water. The data extracted in Figure 7 show that at the superheat temperature difference of 16.97 K the heat flux increased by 1094 kW/m² and the heat transfer coefficient increased by 70.4 kW/m²K. This increase in HTC and CHF values has other impacts in addition to the effect of increasing the density of nucleation sites and roughness in delaying the critical heat flux. The volume of each bubble is equal to the amount of fluid in the micro-layer of the bubble; as the fluid in the micro-layer evaporates and dries, the bubble separates from the surface and moves upwards by overcoming all the forces of weight and surface tension. By creating regular micro-grooves in one direction on the boiling surface, these grooves act like capillaries on the surface and in the sub-layer area; via their capillary force, the fluid in the vicinity of the micro-layer area is drawn into the sub-layer and increases the volume. The fluid is layered in the micro-layer, thus delaying the drying of the micro-layer. This method is a kind of surface engineering used to produce higher boiling surface efficiency without the need for excessive costs.

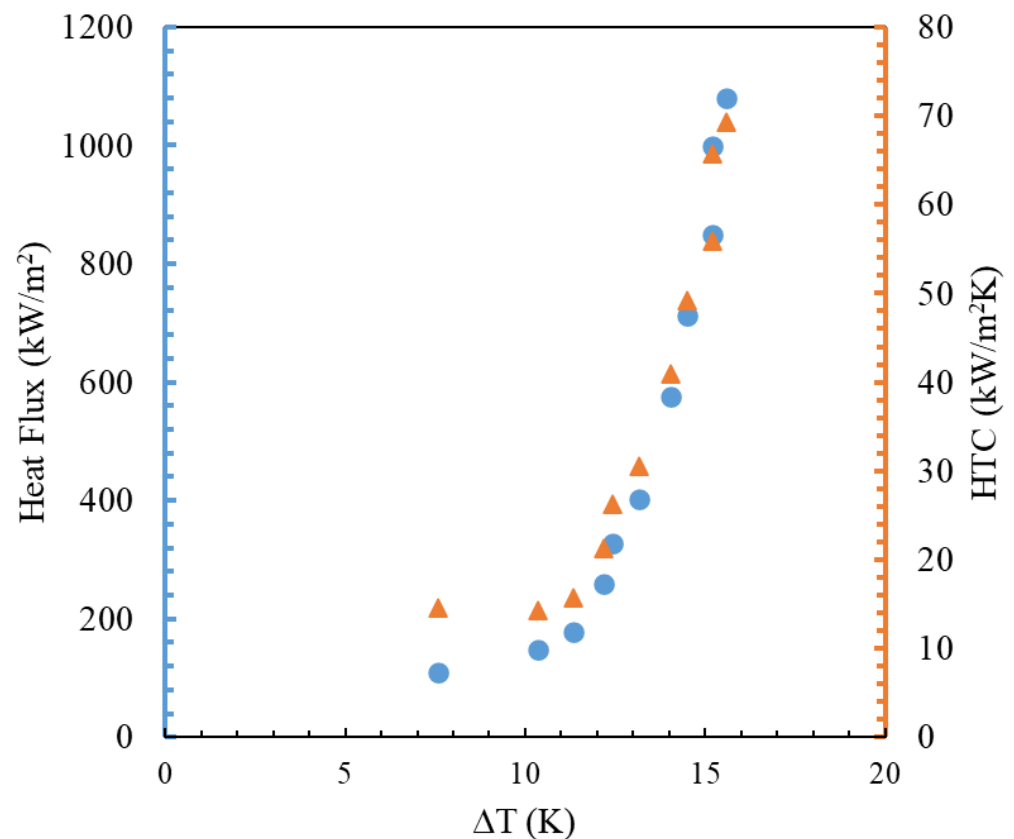


Figure 7. Results of CHF and HTC in ROD.

About 80% of the heat transfer in the boiling process is displaced by the quenching mechanism so that the hot bubble moves out of the sites and active pores of the nucleus act as jet-like fluid and cause the cold fluid above the bubble to move towards these pores—this cooling cycle is always continuous. In fact, the factor that prevented a significant increase in the critical heat flux and heat transfer coefficient upon boiling in the presence of flat surfaces was the collision of a relatively cold downward fluid with hot bubbles coming out of the cavities. To solve this problem, it has been proposed to create a fluid passage path through the vapor by creating a microchannel on the surface by increasing the surface area of the boiling by creating 13 microchannels with a trapezoidal cross-section, as shown in Figure 4d. In microchannels, the temperature at the bottom of the ducts is always higher than the temperature at the tip of the vanes, so the sites at the bottom of the duct are more active than the sites at the edges of the ducts, and most of the bubbles are formed from the bottom of the ducts. These bubbles escape from the center of the channels, and the cold alternating fluid from the sides of the channel feeds the cavities, thus minimizing the collision between the fluid and the bubble.

Also, this jet flow created inside the channels hits the bubbles that are forming on the wall, causing them to burst and increase the bubble production frequency. In the continuation of the boiling process, with increasing heat flux due to the force of evaporation, the bubbles deviate to the center of the channels and produce a cycle and rotational mechanism that causes the bubble and the fluid to separate and not collide. Due to the sum of these factors at the microchannel level, the critical heat flux, as seen in Figure 8, reaches 1826, and the heat transfer coefficient, in Figure 8, reaches 140 at the superheat temperature difference of 12.98 K. The difference in surface temperature indicates an extraordinary increase in the microchannel surface efficiency compared to smooth surfaces. In the images taken from polished surfaces against microchannels, it is clear that in low heat fluxes the bubble production rate on microchannel surfaces was higher than on smooth surfaces. Also, by increasing the heat flux in smooth surfaces, smaller bubbles are quickly connected to

each other and produce larger bubbles, while microchannel surfaces have the ability to have higher heat fluxes and prevent small bubble collisions and the production of larger bubbles.

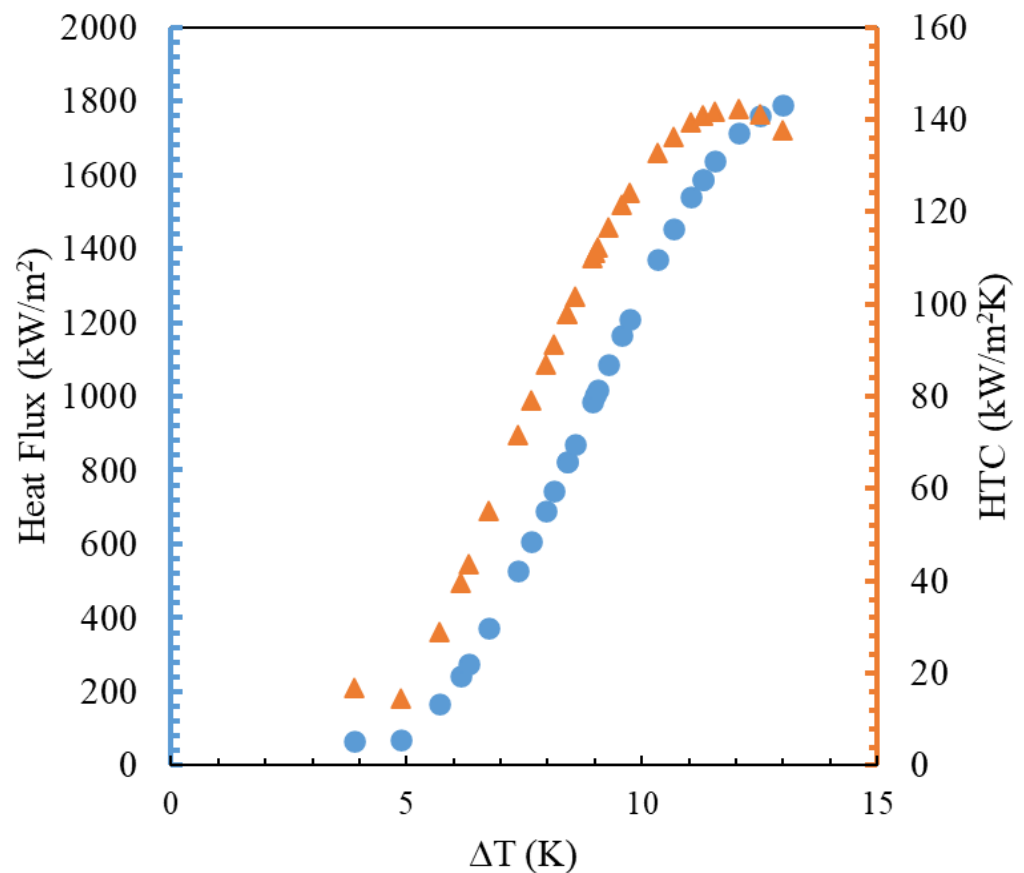


Figure 8. Results of CHF and HTC in microchannel.

Also, with increasing heat flux in the microchannels, the bubbles deflect inward, while the edges of the channels have no bubbles, and these bubbles collide in the center of the microchannels and merge to form a dominant bubble. This dominant bubble continues to grow by swallowing other tiny bubbles until it reaches a critical diameter and is separated from the surface via a buoyant force. By increasing the size of the bubbles, which depends on the increase in heat flux, in the phase of separation of the dominant bubble from the boiling surface, a rising phenomenon is created downstream of the bubble, which leads to faster integration of small bubbles on the surface and the production of another dominant bubble. The phenomenon of bubble burst and turbulence downstream of the ascending bubble causes the adjacent cold fluid to be drawn close to the boiling surface and the surface to be cooled. In fact, this phenomenon indicates the existence of a cooling cycle around the microchannel towards the center of the channels, which causes the separation of the ascending bubble from the descending fluid and is one of the factors increasing HTC and CHF. Due to the total presence of these cooling cycles and the momentary force of bubble evaporation around the fins, the temperature at the surface of the fins did not increase much, despite the large increase in the heat flux.

Finally, by plotting the heat flux diagram in terms of the difference between the superheat temperature and the heat transfer coefficient of all four surfaces according to Figure 9a,b, it is determined that by increasing the efficiency and optimizing the surface the diagram tends to the left and the critical heat flux rarely occurs in low superheat temperature differences. In Figure 9a, the microchannel surface boiling diagram shows that, compared to other flat surfaces, the microchannel surface at a lower heat flux shows higher CHF due to the production of more bubbles at the same superheat temperature.

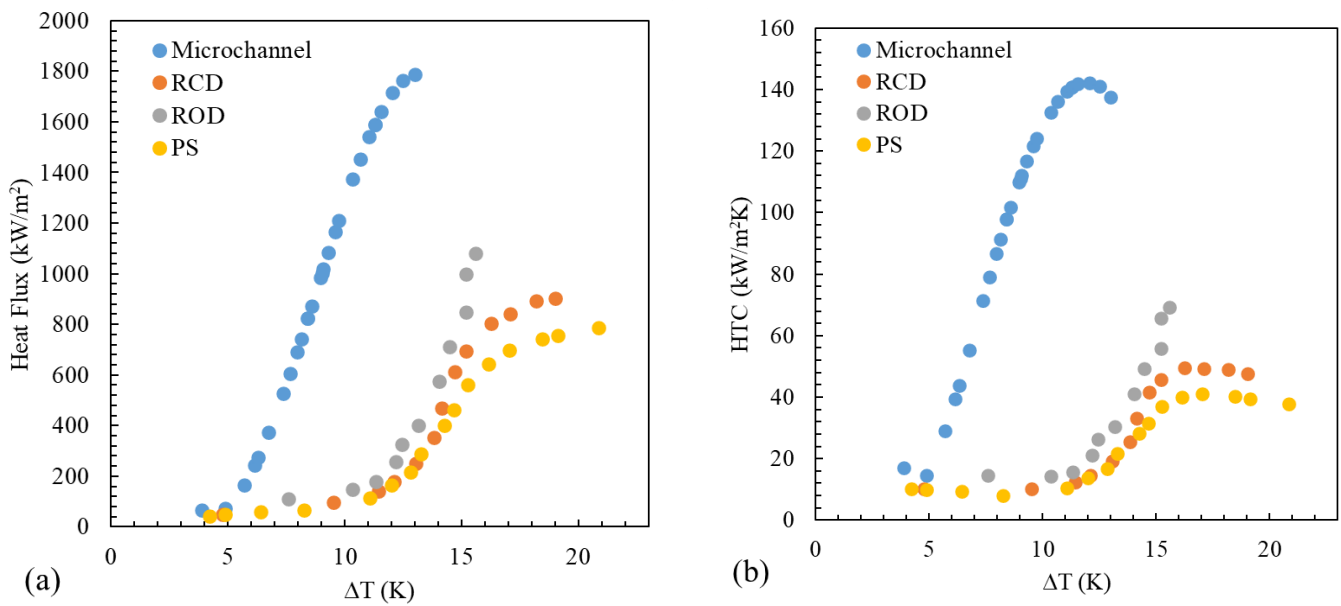


Figure 9. Comparison of all surfaces' CHF (a) and HTC (b).

Also, Table 2 presents a comparative result of all four cases in the given data points.

Table 2. Comparing the results of all cases.

Surface Type	Ra (μm)	ΔT ($^{\circ}\text{C}$)	HTC ($\text{kW}/\text{m}^2 \text{K}$)	CHF (W/m^2)
PS	0.06	20.23	44.5	791,060
RCD	0.170	18.84	53.2	903,746.7
ROD	0.116	16.97	70.4	1,094,243
Microchannel	-	13.02	141.6	1,825,798

4. Conclusions

In this experiment, the effects of four different orientations of the polished surface (PS), the rough surface in a circle (RCD), the rough surface in one direction (ROD), and the microchannel have been investigated. The perfectly polished surface achieves a CHF of 791 kW/m² and an HTC of 44.5 kW/m²K at a surface temperature difference of 20.23 $^{\circ}\text{C}$. By roughening the surface in a circle, and by increasing the roughness and nucleation sites, the heat flux increased by 14.4% and the heat transfer coefficient increased by 17.7% compared to the polished surface. Also, by creating roughness in one direction, in addition to roughening the surface, it helped to feed more micro-layers under the bubble and nucleation sites via capillary channels. In this case, larger bubbles are created. By creating bubbles with a larger diameter, the movement of such bubbles upwards moves a larger volume of cold fluid above the bubble to the boiling surface, and heat transfer increases. The heat flux on this surface increased by 38.6% and the heat transfer coefficient by 55.5% compared to the initial polished surface. It is important to note that HTC and CHF can be increased to this extent without incurring high costs and only by engineering the roughness orientation. Also, by creating a microchannel on the surface, in addition to the fluid on the surface by combining the method of feeding the bubble sub-layer and separating the descending fluid from the rising hot bubble, the bubble path is separated from the surface. In this case, the CHF increased by 131% and the heat transfer coefficient by up to 211%, compared to the polished surface condition.

Funding: This research received no external funding, and the APC was funded by Al-Noor University.

Data Availability Statement: The data presented in this study are available on request from the corresponding author.

Acknowledgments: The author would like to thank Al-Noor University for supporting this work.

Conflicts of Interest: The author declares no conflicts of interest.

Nomenclature

H	Heat transfer coefficient ($W/m^2 K$)
F_{pr}	Pressure correction coefficient
K	Thermal conductivity (W/mK)
P	Pressure (Pa)
Pr	Prandtl number
q''	Heat flux (W/m^2)
R_a	Mean roughness (μm)
T	Temperature (K)
U	Uncertainty
Z	Thermocouples' placement in the heater cartridge (mm)
Greek letters	
μ	Viscosity (N/m^2)
ρ	Density ($kg m^{-3}$)
σ	Surface tension ($N m^{-1}$)
Subscripts	
cr	Critical
l	Liquid
S	Boiling surface
sat	Saturation
v	Vapor

References

- Godinez, J.C.; Cho, H.; Fadda, D.; Lee, J.; Park, S.J.; You, S.M. Effects of materials and microstructures on pool boiling of saturated water from metallic surfaces. *Int. J. Therm. Sci.* **2021**, *165*, 106929. [[CrossRef](#)]
- Alimoradi, H.; Shams, M. Numerical simulation of the effects of surface roughness on nucleation site density of nanofluid boiling. *Modares Mech. Eng.* **2019**, *19*, 1613–1622.
- Chu, H.; Yu, X.; Jiang, H.; Wang, D.; Xu, N. Progress in enhanced pool boiling heat transfer on macro-and micro-structured surfaces. *Int. J. Heat Mass Transf.* **2023**, *200*, 123530. [[CrossRef](#)]
- Mukherjee, S.; Mishra, P.C.; Chaudhuri, P.; Ali, N.; Ebrahim, S.A. Nucleate pool boiling performance of water/titania nanofluid: Experiments and prediction modeling. *Phys. Fluids* **2021**, *33*, 112007. [[CrossRef](#)]
- Alimoradi, H.; Shams, M.; Ashgriz, N. Bubble behavior and nucleation site density in subcooled flow boiling using a novel method for simulating the microstructure of surface roughness. *Korean J. Chem. Eng.* **2022**, *39*, 2945–2958. [[CrossRef](#)]
- Cai, J.; Gong, Z.; Tan, B. Experimental and theoretical investigation of bubble dynamics on vertical surfaces with different wettability for pool boiling. *Int. J. Therm. Sci.* **2023**, *184*, 107966. [[CrossRef](#)]
- Khodadadi, S.; Taleghani, M.H.; Ganji, D.D.; Gorji-Bandpy, M. Heat transfer enhancement via bubble dynamics along an inclined wall. *Int. Commun. Heat Mass Transf.* **2023**, *145*, 106829. [[CrossRef](#)]
- Alimoradi, H.; Shams, M.; Valizadeh, Z. The effects of nanoparticles in the subcooled boiling flow in the channels with different cross-sectional area and same hydraulic diameter. *Modares Mech. Eng.* **2017**, *16*, 545–554.
- Abdulkadhim, A.; Hamzah, H.K.; Ali, F.H.; Abed, A.M.; Abed, I.M. Natural convection among inner corrugated cylinders inside wavy enclosure filled with nanofluid superposed in porous–nanofluid layers. *Int. Commun. Heat Mass Transf.* **2019**, *109*, 104350.
- Zhang, L.; Gong, S.; Lu, Z.; Cheng, P.; Wang, E.N. A unified relationship between bubble departure frequency and diameter during saturated nucleate pool boiling. *Int. J. Heat Mass Transf.* **2021**, *165*, 120640. [[CrossRef](#)]
- Alimoradi, H.; Shams, M.; Ashgriz, N. Enhancement in the pool boiling heat transfer of copper surface by applying electrophoretic deposited graphene oxide coatings. *Int. J. Multiph. Flow* **2023**, *159*, 104350. [[CrossRef](#)]
- Kim, M.; Kim, S.J. A mechanistic model of critical heat flux for pool boiling based on supply failure mechanisms depending on the contact angle. *Int. J. Heat Mass Transf.* **2023**, *209*, 124090. [[CrossRef](#)]
- Ghanavati, A.; Khodadadi, S.; Taleghani, M.H.; Gorji-Bandpy, M.; Ganji, D.D. Numerical simulation of the motion and interaction of bubble pair rising in a quiescent liquid. *Appl. Ocean Res.* **2023**, *141*, 103769. [[CrossRef](#)]

14. Eskandari, E.; Alimoradi, H.; Pourbagian, M.; Shams, M. Numerical investigation and deep learning-based prediction of heat transfer characteristics and bubble dynamics of subcooled flow boiling in a vertical tube. *Korean J. Chem. Eng.* **2022**, *39*, 3227–3245. [[CrossRef](#)]
15. Barathula, S.; Alapati, J.K.; Srinivasan, K. Investigation of acoustic spectral variations in the pool boiling regimes of water on wire heater. *Appl. Therm. Eng.* **2023**, *226*, 120281. [[CrossRef](#)]
16. Alimoradi, H.; Shams, M. Optimization of subcooled flow boiling in a vertical pipe by using artificial neural network and multi objective genetic algorithm. *Appl. Therm. Eng.* **2017**, *111*, 1039–1051. [[CrossRef](#)]
17. Mahmoud, M.M.; Karayiannis, T.G. Bubble growth models in saturated pool boiling of water on a smooth metallic surface: Assessment and a new recommendation. *Int. J. Heat Mass Transf.* **2023**, *208*, 124065. [[CrossRef](#)]
18. Abdulkadhim, A.; Hamzah, H.K.; Ali, F.H.; Yıldız, Ç.; Abed, A.M.; Abed, E.M.; Arıcı, M. Effect of heat generation and heat absorption on natural convection of Cu-water nanofluid in a wavy enclosure under magnetic field. *Int. Commun. Heat Mass Transf.* **2021**, *120*, 105024. [[CrossRef](#)]
19. Hu, X.; Derakhshanfard, A.H.; Patra, I.; Khalid, I.; Jalil, A.T.; Opulencia, M.J.; Dehkordi, R.B.; Toghraie, D.; Hekmatifar, M.; Sabetvand, R. The microchannel type effects on water-Fe₃O₄ nanofluid atomic behavior: Molecular dynamics approach. *J. Taiwan Inst. Chem. Eng.* **2022**, *135*, 104396. [[CrossRef](#)]
20. Fan, S.; Jiao, L.; Wang, K.; Duan, F. Pool boiling heat transfer of saturated water on rough surfaces with the effect of roughening techniques. *Int. J. Heat Mass Transf.* **2020**, *159*, 120054. [[CrossRef](#)]
21. Musavi, S.H.; Adibi, H.; Rezaei, S.M. An experimental study on bubble dynamics and pool boiling heat transfer of grinding/laser-structured surface. *Heat Mass Transf.* **2023**, *59*, 681–698. [[CrossRef](#)]
22. Taleghani, M.H.; Khodadadi, S.; Maddahian, R.; Mokhtari-Dizaji, M. Enhancing the bubble collapse energy using the electrohydrodynamic force. *Phys. Fluids* **2023**, *35*, 053316. [[CrossRef](#)]
23. Singh, S.K.; Sharma, D. Experimental Investigation on Pool Boiling Heat Transfer Performance of Superhydrophilic, Hydrophilic and Hydrophobic Surface. *Int. J. Thermophys.* **2024**, *45*, 53. [[CrossRef](#)]
24. Alimoradi, H.; Eskandari, E.; Pourbagian, M.; Shams, M. A parametric study of subcooled flow boiling of Al₂O₃/water nanofluid using numerical simulation and artificial neural networks. *Nanoscale Microscale Thermophys. Eng.* **2022**, *26*, 129–159. [[CrossRef](#)]
25. Abed, A.M.; Sopian, K.; Mohammed, H.A.; Alghoul, M.A.; Ruslan, M.H.; Mat, S.; Al-Shamani, A.N. Enhance heat transfer in the channel with V-shaped wavy lower plate using liquid nanofluids. *Case Stud. Ther. Eng.* **2015**, *5*, 13–23. [[CrossRef](#)]
26. Li, W.; Dai, R.; Zeng, M.; Wang, Q. Review of two types of surface modification on pool boiling enhancement: Passive and active. *Renew. Sustain. Energy Rev.* **2020**, *130*, 109926. [[CrossRef](#)]
27. Cooke, D.; Kandlikar, S.G. Effect of open microchannel geometry on pool boiling enhancement. *Int. J. Heat Mass Transf.* **2012**, *55*, 1004–1013. [[CrossRef](#)]
28. Sangeetha, A.; Shanmugan, S.; Alrubaie, A.J.; Jaber, M.M.; Panchal, H.; Attia, M.E.; Elsheikh, A.H.; Mevada, D.; Essa, F.A. A review on PCM and nanofluid for various productivity enhancement methods for double slope solar still: Future challenge and current water issues. *Desalination* **2023**, *551*, 116367. [[CrossRef](#)]
29. Mehralizadeh, A.; Shabaniyan, S.R.; Bakeri, G. Effect of modified surfaces on bubble dynamics and pool boiling heat transfer enhancement: A review. *Therm. Sci. Eng. Prog.* **2020**, *15*, 100451. [[CrossRef](#)]
30. Mahmoud, M.M.; Karayiannis, T.G. Pool boiling review: Part II—Heat transfer enhancement. *Therm. Sci. Eng. Prog.* **2021**, *25*, 101023. [[CrossRef](#)]
31. Shahnazari, M.R.; Esfandiari, M. Capillary Effects on Surface Enhancement in a Non-Homogeneous Fibrous Porous Medium. *Mech. Adv. Compos. Struct.* **2018**, *5*, 83–90.
32. Mori, S.; Utaoka, Y. Critical heat flux enhancement by surface modification in a saturated pool boiling: A review. *Int. J. Heat Mass Transf.* **2017**, *108*, 2534–2557. [[CrossRef](#)]
33. Abdollahi, A.; Salimpour, M.R.; Etesami, N. Experimental analysis of pool boiling heat transfer of ferrofluid on surface deposited with nanofluid. *Modares Mech. Eng.* **2016**, *16*, 19–30.
34. Berenson, P.J. Experiments on pool boiling heat transfer. *Int. J. Heat Mass Transf.* **1962**, *5*, 985–999. [[CrossRef](#)]
35. Jones, B.J.; McHale, J.P.; Garimella, S.V. The influence of surface roughness on nucleate pool boiling heat transfer. *ASME J. Heat Mass Transf.* **2009**, *131*, 253. [[CrossRef](#)]
36. Jacob, M.; Fritz, W. Experiments on the evaporation process. *Res. Eng.* **1931**, *2*, 435–447.
37. Ramilson, J.M.; Sadasivan, P.; Hard, J.H.L. Surface factor influencing burnout on flat heaters. *Heat Transf.* **1992**, *114*, 287–290. [[CrossRef](#)]
38. Al-Farhany, K.; Abdulkadhim, A.; Hamzah, H.K.; Ali, F.H.; Chamkha, A. MHD effects on natural convection in a U-shaped enclosure filled with nanofluid-saturated porous media with two baffles. *Prog. Nucl. Energy* **2022**, *145*, 104136. [[CrossRef](#)]
39. Kumar, N.; Ghosh, P.; Shukla, P. Effect of composite coatings on surface characteristics and boiling heat transfer performance in a pool of water. *J. Therm. Anal. Calorim.* **2024**, *149*, 671–685. [[CrossRef](#)]
40. Wang, C.Y.; Ji, W.T.; Zhao, C.Y.; Chen, L.; Tao, W.Q. Experimental determination of the role of roughness and wettability on pool-boiling heat transfer of refrigerant. *Int. J. Refrig.* **2023**, *153*, 205–221. [[CrossRef](#)]
41. Dehkordi, K.G.; Karimipour, A.; Afrand, M.; Toghraie, D.; Isfahani, A.H.M. Molecular dynamics simulation concerning nanofluid boiling phenomenon affected by the external electric field: Effects of number of nanoparticles through Pt, Fe, and Au microchannels. *J. Mol. Liq.* **2021**, *324*, 114775. [[CrossRef](#)]

42. Souza, R.R.; Passos, J.C.; Cardoso, E.M. Influence of nanoparticle size and gap size on nucleate boiling using HFE7100. *Experimental Therm. Fluid Sci.* **2014**, *59*, 195–201. [[CrossRef](#)]
43. Gheitaghy, A.M.; Saffari, H.; Shendi, J.S. Pool boiling enhancement by electrodeposited porous micro/nanostructured on copper surface. *Modares Mech. Eng.* **2015**, *15*, 159–167.
44. Narayan, G.P.; Anoop, K.B.; Das, S.K. Mechanism of enhancement/deterioration of boiling heat transfer using stable nano-particle suspensions over vertical tubes. *J. Appl. Phys.* **2007**, *102*, 74317. [[CrossRef](#)]
45. Vafaei, S. Nanofluid pool boiling heat transfer phenomenon. *J. Powder Technol.* **2015**, *277*, 181–192. [[CrossRef](#)]
46. Ahmed, O.; Hamed, M.S. Experimental investigation of the effect of particle deposition on pool boiling of nanofluid. *Int. J. Heat Mass Transf.* **2012**, *55*, 3423–3436. [[CrossRef](#)]
47. Gheitaghy, A.M.; Saffari, H.; Mohebbi, M. Investigation pool boiling heat transfer in U shaped mesochannel with electrode-posed porous coating. *Exp. Therm. Fluid Sci.* **2016**, *79*, 87–97. [[CrossRef](#)]
48. Jaikumar, A.; Kandlikar, S.G. Enhanced pool boiling heat transfer mechanisms for selectively sintered open microchannels. *Int. J. Heat Mass Transf.* **2015**, *88*, 652–661. [[CrossRef](#)]
49. Moffat, R.J. Describing the uncertainties in experimental results. *Exp. Therm. Fluid Sci.* **1988**, *1*, 3–17. [[CrossRef](#)]
50. Mourgues, A.; Hourtane, V.; Muller, T.; Charles, M.C. Boiling behaviors and critical heat flux on a horizontal and vertical plate in saturated pool boiling with and without ZnO nanofluid. *Int. J. Heat Mass Transf.* **2013**, *57*, 595–606. [[CrossRef](#)]
51. Táboas, F.; Valles, M.; Bourouis, M.; Coronas, A. Pool boiling of ammonia/water and its pure components: Comparison of experimental data in the literature with the predictions of standard correlations. *Int. J. Refrig.* **2007**, *30*, 778–788. [[CrossRef](#)]
52. Das, S.; Bhaumik, S. Experimental study of nucleate pool boiling heat transfer using water on thin-film surface. *Iran J. Sci. Technol. Trans. Mech. Eng.* **2016**, *40*, 21–29. [[CrossRef](#)]
53. Sarafraz, M.M.; Kiani, T.; Hrmozi, F. Critical heat flux and pool boiling heat transfer analysis of synthesized zirconia aqueous nanofluid. *Int. Commun. Heat Mass Transf.* **2016**, *70*, 75–83. [[CrossRef](#)]
54. Kiyomura, I.S.; Manetti, L.L.; da Cunha, A.P.; Ribatski, G.; Cardoso, E.M. An analysis of nanoparticles deposition on characteristics of the heating surface and on pool boiling of water. *Int. J. Heat Mass Transf.* **2017**, *106*, 666–674. [[CrossRef](#)]

Disclaimer/Publisher’s Note: The statements, opinions and data contained in all publications are solely those of the individual author(s) and contributor(s) and not of MDPI and/or the editor(s). MDPI and/or the editor(s) disclaim responsibility for any injury to people or property resulting from any ideas, methods, instructions or products referred to in the content.